

High Resolution FUV Spectroscopy of the Terrestrial Day Airglow with FUSE

Paul D. Feldman, David J. Sahnou, Jeffrey W. Kruk, Edward M. Murphy¹, and H. Warren Moos

Department of Physics and Astronomy, The Johns Hopkins University
Charles and 34th Streets, Baltimore, Maryland 21218

Abstract.

During orbital verification, the Far Ultraviolet Spectroscopic Explorer (FUSE) obtained spectra of the terrestrial day airglow between 905 and 1184 Å from an altitude of 766 km. The spectrographs have three apertures that can simultaneously record the atmospheric emissions with limiting instrumental spectral resolutions of approximately 0.4, 0.05, and 0.03 Å. Seven orbits were obtained of observations of the sunlit Earth and disclose a wealth of emissions resulting from the electron impact excitation of N₂ in addition to emissions of O I, N I, and N II produced by both photoelectron impact and by photodestructive excitation and ionization of thermospheric O and N₂ by extreme ultraviolet solar radiation. The argon resonance transitions are unambiguously identified as are previously unreported transitions between highly excited energy levels of O⁺. These spectra have the highest spectral resolution and sensitivity in this spectral range to date and will provide valuable input to the interpretation of lower resolution spectra from current and future Earth remote sensing missions.

INTRODUCTION

Ultraviolet spectroscopy of the terrestrial upper atmosphere has long been recognized as an important tool in determining the compositional varia-

tion and thermal structure of the atmosphere above 100 km and of understanding the response of the atmosphere to varying solar electromagnetic and particle radiation. An excellent overview of the subject has been presented by *Meier* [1991]. Observations from both sounding rockets, which enable vertical sounding of the atmosphere [*Gentieu*

¹Present address: Department of Astronomy, P. O. Box 3818, University of Virginia, Charlottesville, VA 22903

et al., 1979, 1981], and satellites, which provide global and long-term monitoring [Chakrabarti et al., 1983], have typically measured spectra in the 400–1200 Å wavelength band at spectral resolutions of 4–8 Å. A few rocket experiments have flown spectrographs with resolutions of 1–2 Å [Christensen et al., 1982; Morrison et al., 1990], but these have had limited success because of the relatively low signal-to-noise ratio resulting from small instrumental effective area and short observation times. Moreover, even this resolution is insufficient to sort out the rich emission spectrum resulting primarily from photoelectron impact and photodestructive processes involving the principal constituents of the thermosphere, molecular nitrogen and atomic oxygen.

In the far ultraviolet, astronomical observatories in low-Earth orbit, when observing during orbit day, must contend with a large number of emissions that blanket the spectral region, much as the night sky emissions of OH in the near infrared contaminate spectra obtained by ground-based telescopes. Yet these missions also provide opportunities to study the terrestrial airglow with unprecedented sensitivity and spectral resolution. For example, the Hopkins Ultraviolet Telescope (HUT), which flew on the *Astro-1* and 2 space shuttle missions in December 1990 and March 1995, respectively, produced excellent spectra at 3.3 Å resolution, looking both upward and down at the bright Earth. These data remain largely unpublished [Feldman et al., 1991, 1992]. With FUSE, using the low resolution aperture (LWRS, 30" × 30"), the spectral resolution is a factor of ten better than that of HUT, and the medium resolution aperture (MDRS, 4" × 20") is capable of a further factor of 7.5 [Moos et al., 2000]. A third, high resolution aperture (HIRS, 1."25 × 20"), has lower throughput but only marginally better spectral resolution because corrections for image curvature have not yet been implemented. The dayglow is recorded simultaneously in all three aper-

tures.

In this paper, we present an atlas of spectra of the illuminated Earth taken with the medium resolution aperture during Orbital Verification. The spectra were taken with the spectrographs not in final focus, and some degradation in spectral resolution results from thermally induced rotations of the gratings [Sahnow et al., 2000]. Nevertheless, the wealth of detail revealed makes possible the resolution of some current problems in aeronomy and provides sensitive tests of current radiative transfer models. Some examples are given below, although detailed modeling is beyond the scope of the present paper.

OBSERVATIONS

The bright earth airglow spectra are a combination of 7 photon list (time-tagged) observations taken between 17:40 UT on September 24, 1999 and 04:20 UT on September 25, 1999. The individual spectra were obtained during 7 consecutive bright earth occultations of a fixed celestial pointing towards an empty field. The telescope line-of-sight described a chord across the fully illuminated disk making a minimum angle of $\sim 34^\circ$ with respect to the satellite nadir (from the FUSE orbit of 766 km, the earth subtends a half angle of 63.2°). Direct downward viewing is prohibited by constraints on the telescope look direction relative to the orbital velocity vector. During each occultation, spectra were accumulated not only of the bright disk but also of the emissions from the Earth's limb. Since the data were accumulated in time-tagged mode, it was possible to separate out the spectra of the disk and the limb, and, in the case of the latter, to extract limb profiles with a spatial resolution of ~ 20 km (the LWRS aperture subtends less than 1 km at a tangent height of 200 km so that higher spatial resolution is possible albeit with a corresponding loss in S/N). The disk spectrum presented below is the accumulation of

11,477 seconds of bright Earth data and has a sufficient signal-to-noise ratio in MDRS mode to be useful as a spectral atlas. Because of the larger throughput, spectra from the LWRS are used for the determination of absolute brightnesses and the extraction of limb profiles. Spectra cover the range 905–1184 Å.

These data were taken with Detector 1 as the high voltage of Detector 2 was turned off at the time of the observation. *Sahnow et al.* [2000] have identified an unusual calibration problem in the long wavelength segment (>1155 Å) of Detector 1. Focussed starlight at long wavelengths is occulted by a repeller wire located close to the tangential focus of the grating. This leads to erroneously low values of the system effective area derived from measurements of standard white dwarf stars that are used for the absolute flux calibration used in the pipeline processing of the data. However, this effect is negligible for extended sources filling the aperture such as airglow. To evaluate the correction required for the airglow, we use a cross comparison of four orbits of bright Earth observations made on March 27, 2000 with both detectors operating. This latter data set has limited local time coverage and much shorter total integration time (4,572 seconds) and so is much less appropriate to the extraction of nadir intensities and limb profiles. All of the data were processed with absolute flux calibration in use as of August 18, 2000.

For comparison, we will also refer to side-looking airglow spectra (in fact, the viewing angle is actually close to 90° from the local zenith) that are derived from $\sim 20,000$ seconds worth of photon list data taken on August 15 and 16, 1999, during 20 separate exposures obtained during detector characterization tests. The aperture was positioned at apparent right ascension $7^h 6^m 57^s$ and declination $-65^\circ 0' 59''$ (equinox J2000) throughout these exposures. Once again, only data from Detector 1 was obtained at this time. The August

and September 1999 observations were obtained at a time of moderate solar activity ($F_{10.7} \approx 130$) while $F_{10.7} \approx 205$ for the March 2000 observation.

SPECTRA

Figures 1 through 4 show MDRS spectra of the bright Earth from the SiC1 and LiF1 channels of Detector 1. In the region of overlap of the SiC and LiF channels, only the higher S/N LiF data are presented, except in the 1081–1090 Å gap between the two LiF segments where the important N II $\lambda 1085$ multiplet falls. For the spectral region longward of 1100 Å, due to the calibration uncertainty of the LiF1 detector and the higher throughput of Detector 2, data from the LiF2 detector from March 27, 2000, are shown in Figures 5 and 6. The effective spectral resolution is determined by fitting gaussians to the several strong isolated atomic lines in the LiF spectra and is found to lie in the range of 0.07–0.08 Å. This is larger than the instrumental width expected for the $4''$ wide MDRS slit, and is attributed to thermal distortion of the optical bench over the course of the observations that is not completely compensated for in the pipeline processing and the fact that the spectral curvature due to astigmatism is not removed.

Wavelength identifications of the atomic features are from *Morton* [1991] and *Kelly* [1987] while the N₂ band identifications are from the medium and high resolution laboratory spectra of *Ajello et al.* [1989] and *Ajello et al.* [1998], respectively. High resolution laboratory spectroscopy of the N₂ $c_4' - X(0,0)$ band, under optically thin conditions, is presented by *Shemansky et al.* [1995]. This band has a very large electron excitation cross-section but is extremely weak in the terrestrial airglow due to predissociation loss and branching to other more optically thin transitions during repeated cycles of absorption and emission of individual lines. This problem has been treated theoretically in detail by *Stevens et al.* [1994] de-

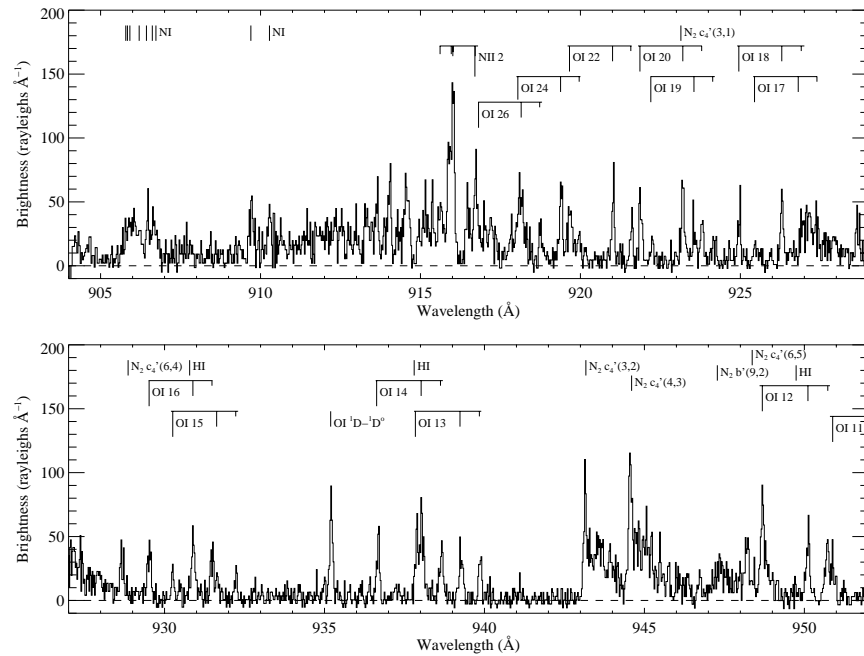


Figure 1. FUSE MDRS spectrum of the illuminated disk of the Earth as observed in September 1999. The data are from the SiC1 channel and span 904–952 \AA . Atomic and molecular features are identified in the figure.

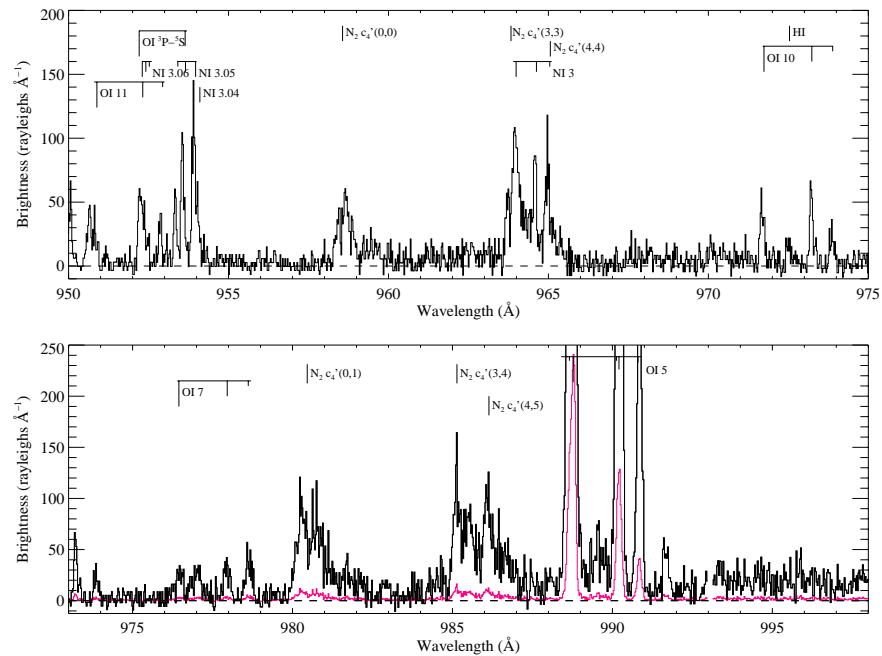


Figure 2. Figure 1 continued. The red line represents the data divided by 10. The data are from the SiC1 channel and span 950–993 \AA . From 993–998 \AA the data are from the LiF1 channel.

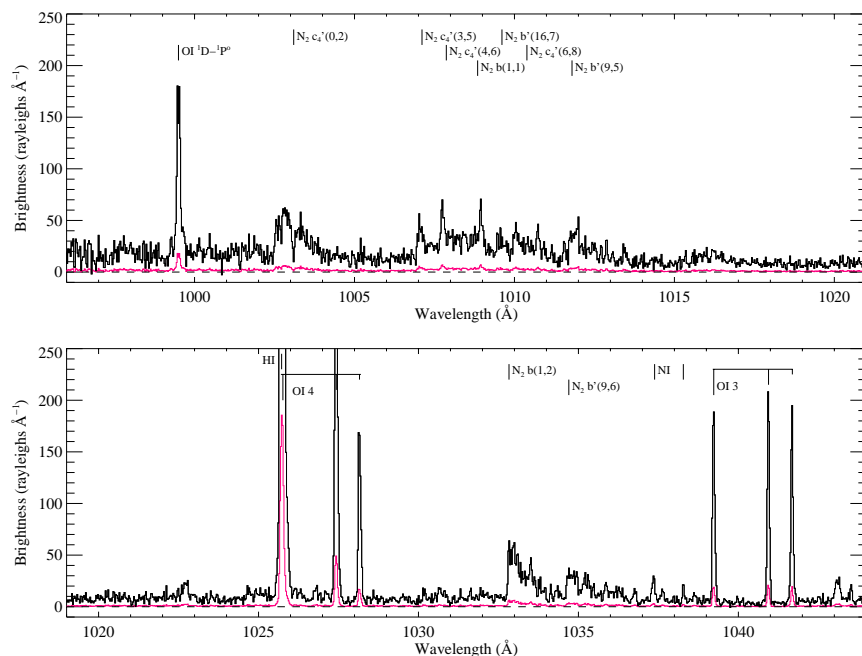


Figure 3. Figure 1 continued. The data are from the LiF1 channel and span 996–1044 Å.

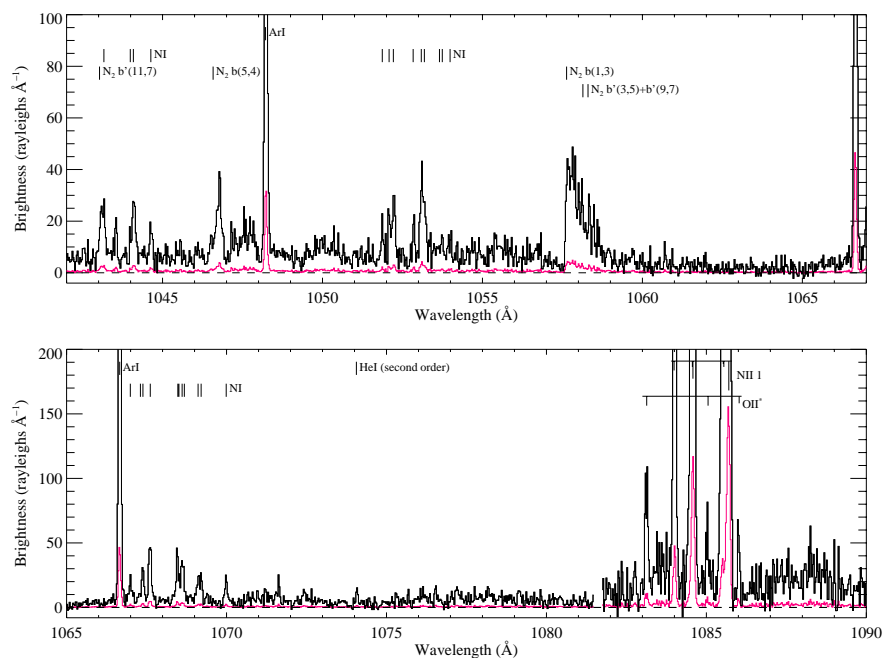


Figure 4. Figure 1 continued. The data are from the LiF1 channel and span 1042–1081 Å. From 1082–1090 Å the data are from the SiC1 channel.

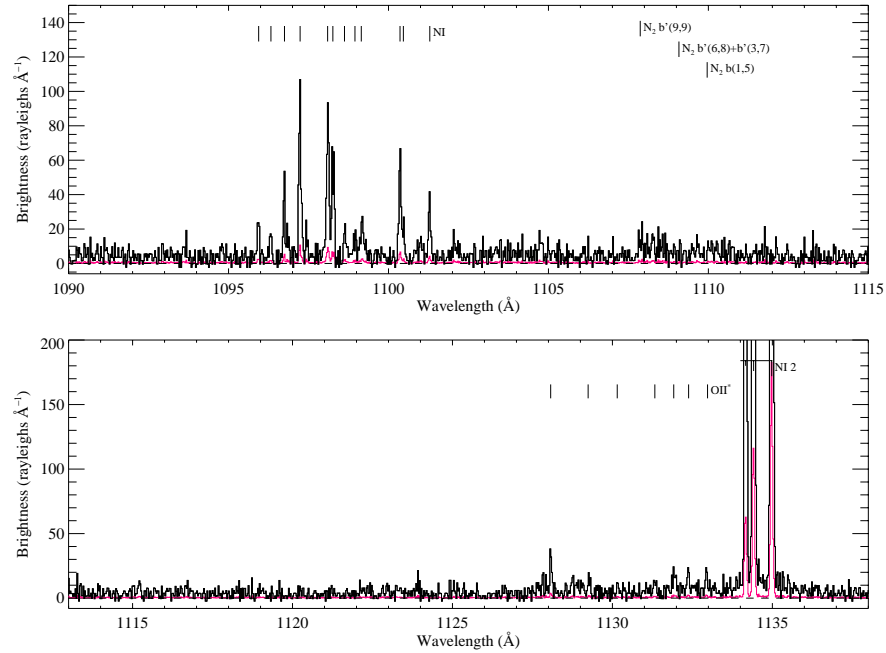


Figure 5. FUSE MDRS spectrum of the illuminated disk of the Earth as observed in March 2000. The data are from the LiF2 channel and span 1090–1138 Å.

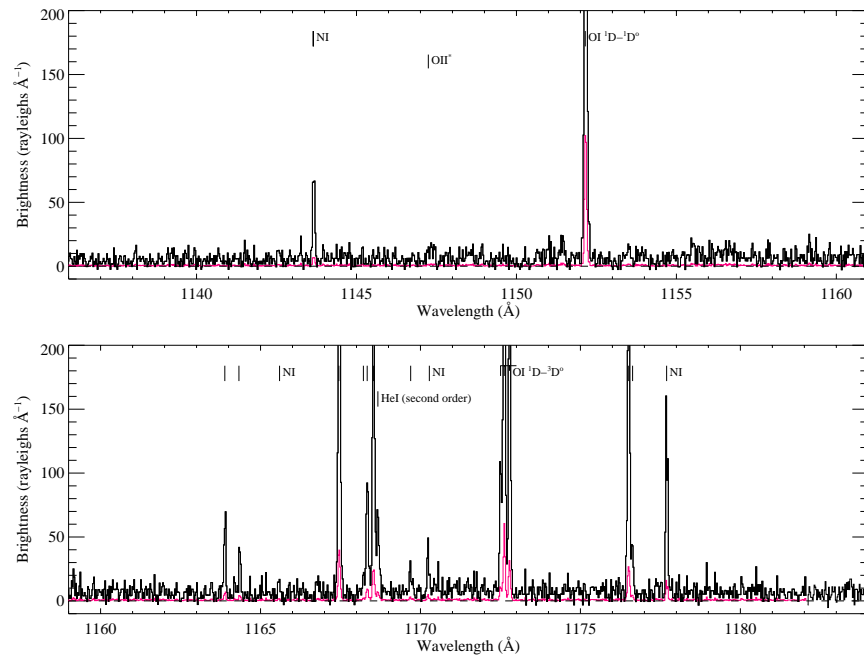


Figure 6. Figure 5 continued. The data are from the LiF2 channel and span 1136–1184 Å.

spite the paucity of observational data. In the figures, the N_2 bands are indicated by the positions of the R-branch origins taken from *Ajello et al.* [1989, 1998] and with further identifications from the tables of *Roncin and Launay* [1998]. In Figure 1 additional O I lines below 916 Å are not explicitly identified. Note that the H I Lyman series is relatively weak in the disk spectra, as is the geocoronal He I $\lambda 584$ line seen in second order at 1168 Å. These lines are considerably stronger in the limb and side-looking airglow spectra.

In Figure 4, two of the strongest features are the resonance transitions of Ar I at 1048 and 1067 Å. These features are present in the HUT spectra of the bright Earth at comparable brightness [*Feldman et al.*, 1991], but the spectral resolution of FUSE makes possible the clean separation of the Ar I lines from nearby N_2 and N I emissions. Both lines show limb darkening that would be expected from a low altitude source attenuated by an absorber with a smaller scale height above the homopause, in this case O_2 . At these wavelengths the vertical optical depth of O_2 reaches unity at ~ 90 km at which altitude the vertical optical depth at the center of the Ar I transitions is greater than 10^4 [*Parker et al.*, 1998], so that a full radiative transfer analysis is required to understand the variation in brightness with viewing geometry.

An even more striking illustration of the power of the high spectral resolution of these data is the identification in Figure 4 of three satellite features near the resolved components of the N II $\lambda 1085$ multiplet. These three lines form a multiplet connecting the excited $(2s2p^4) ^4P$ state of O^+ (the upper level of the O II $\lambda 834$ resonance transition) to the $(2s^22p^23p) ^4S^o$ state that lies 26.3 eV above the O^+ ground state [*Pettersson and Wernaker*, 1990]. Additional transitions from other states of the $(2s^22p^23p)$ configuration to the 4P state are identified in Figures 5 and 6. Assuming the source to be photoionization of atomic oxygen (which, according to *Meier* [1991] produces

over 90% of the excitation of O II $\lambda 834$), the total energy required is 39.9 eV, which is close to and just below the energy of the very strong solar He II $\lambda 304$ line that dominates photoelectron production in the thermosphere. The excited O II multiplet, here designated O II*, accounts for $\sim 6\%$ of the total observed emission at 1085 Å. Although the FUSE spectral range does not include O II $\lambda 834$, the HUT bright Earth spectra, obtained near solar maximum, can be used to estimate a ratio of N II $\lambda 1085$ to O II $\lambda 834$, from which we find that O II* $\lambda 1085$ is about 1% as bright as O II $\lambda 834$.

Table 1 gives the brightnesses of the strongest features derived from the LWRS spectra. To facilitate comparison with models, these are not extracted from the pipeline processed spectra used to generate Figures 1 – 6, but are derived directly from the raw time-tagged data files where the range in local time is limited to from one hour before to one hour after orbital local noon. These are from the September 1999 observations with the corrections for flux calibration at the longest wavelengths described above. Also given in the table are the corresponding brightnesses for the side-looking emissions from the spacecraft altitude of 766 km, extracted for the same time interval around local noon. “Side-looking” in this case is viewing $\sim 90^\circ$ to the local zenith at an angle of 27° above the bright limb. In this case only optically thick emissions of O I and N I are observed in addition to geocoronal H I and He I.

Figure 7 compares the LWRS spectrum from the short wavelength end of the SiC1 channel (905–993 Å) of the limb (top panel) with similar spectra of the disk (middle panel) and the side-looking airglow (bottom panel). The limb spectrum consists of 892 seconds of data with the line-of-sight between 4.9 and 11.1° of the limb, corresponding to tangent heights of 250 to 500 km. The solar zenith angle at the point of observation varies from 59 to 66° . The most striking difference between the limb and disk spectra, other than the rel-

Table 1. Observed Dayglow Brightnesses in the FUSE LWRS aperture. The data are from Detector 1 taken in August and September 1999.

Transition	Wavelength (Å)	Down-looking ^a (rayleighs)	Side-looking ^b (rayleighs)
H I Lyman- δ	950	—	2.4 ± 0.7^c
H I Lyman- γ	973	2.4 ± 0.7	9.0 ± 1.1
O I 5	989	775 ± 17	30 ± 4.2
H I Lyman- β + O I 4	1026	225 ± 8	140 ± 3
O I 4	1027	71 ± 3.0	8.2 ± 0.9
O I 3	1040	63 ± 2.3	2.0 ± 0.5
Ar I 2	1048	37 ± 1.5	—
Ar I 1	1066	49 ± 2.0	—
N II 1	1085	400 ± 13	~ 1
N I 2	1134	290 ± 10	2.5 ± 0.4
O I $^1D - ^1D^o$	1152	110 ± 3.4	—
N I $^2D^o - ^2F$	1167	51 ± 2.7^d	—
O I $^1D - ^3D^o$	1173	105 ± 6.5^d	—
N ₂ $c_4' - X (3,2)+(4,3)$	943	105 ± 3.0	—
N ₂ $c_4' - X (0,0)$	958	30 ± 3.2	—
N ₂ $c_4' - X (0,1)$	981	68 ± 3.8	—
N ₂ $c_4' - X (3,4)+(4,5)$	985	98 ± 4.6	—
N ₂ $c_4' - X (0,2)$	1003	42 ± 2.9	—

^aSeptember 24–25, 1999; local time 1100–1300 hr; solar zenith angle 20–28°; viewing angle 34–42° from nadir; average over seven orbits.

^bAugust 15–16, 1999; local time 1100–1300 hr; solar zenith angle 5–17°; viewing angle 90° from zenith; average over six orbits.

^cIncludes 1- σ statistical uncertainty and orbit-to-orbit variation. The absolute uncertainty is $\pm 10\%$, except for the emissions longward of 1155 Å where the uncertainty is of the order of $\pm 20\%$.

^dCorrected for Detector 1 calibration uncertainty using Detector 2 data from March 27, 2000.

ative strengths of the N₂ and O I emissions, is the presence of the O⁺ + e⁻ recombination continuum below 911 Å in the limb spectrum. This feature was first resolved spectrally by *Feldman et al.* [1992] in HUT/*Astro-1* nighttime observations of a setting target, and has subsequently been reanalyzed by *Meléndez-Alvira et al.* [1999]. Note however, the contamination of the continuum with N I emissions clearly seen in the disk spectrum (see also Figure 1).

LIMB PROFILES

Observations of the ultraviolet airglow emissions as a function of distance (or more appropriately, tangent height) above a planetary limb provide a unique means for testing models of atmospheric composition and excitation mechanisms. Such measurements go back to the early days of the space era yet continue to bear fruit with successive developments in spectroscopic instrumentation [*Gladstone, 1988; Meier, 1991; Budzien et al., 1994*]. In Figures 8 and 9 we give several examples that bear on some recently discussed problems.

O I λ1173/O I λ989 Ratio

The multiplets O I λ1173 and O I λ989 have a common 3s' 3D^o upper state with a laboratory branching ratio of $\sim 1.5 \times 10^{-4}$. An additional branch to 3p 3P occurs at 7990 Å with a comparable but less well known branching ratio. Because the individual lines of the O I λ989 multiplet scatter several thousand times before escaping the atmosphere, the brightness of O I λ1173 becomes significant. This problem has been discussed in detail by both *Gladstone et al.* [1987] and *Morrison and Meier* [1988] who demonstrate that both the altitude profiles of the total radiation in each multiplet as well as the relative intensities of the lines within each multiplet can provide information about the atomic oxygen density as well as

serve as a check on the validity of the radiative transfer models used to analyze the stronger oxygen emissions. The resolution of each multiplet into three components is clearly within the capability of the FUSE MDRS slit as demonstrated in Figures 2 and 6. Limb profiles of these two multiplets are shown in Figures 8a and 8c. The profile for O I λ989 is characteristic of an optically thick profile, being relatively flat up to ~ 300 km and then decreasing slowly with altitude [*Gladstone, 1988*]. Note the change in slope above 400 km tangent height, similar to what was observed in a sounding rocket experiment by *Cotton et al.* [1993], suggestive of a small component of hot thermospheric oxygen [*Hubert et al., 1999*].

In contrast, the O I λ1173 profile is typical of a photoelectron excited optically thin emission with a peak at ~ 180 km and a top side scale height of the emitting atmospheric species. The photoelectron excitation source profile can be deduced from the profile of the optically thin ¹D – ¹D^o transition at 1152 Å, shown in Figure 8d, and gives a top side scale height of ~ 70 km, characteristic of atomic oxygen in diffusive equilibrium at 1000 K. On the other hand, the O I λ1173 profile actually has a smaller top side scale height, ~ 50 km, which may be understood as reflecting the decreasing number of 989 Å photon scatterings with decreasing atmospheric density.

Meier [1991] also cites a calculation of the O I λ1173/O I λ989 brightness ratio looking down from 850 km for solar minimum conditions and a solar zenith angle of 80°, based on the model of *Morrison and Meier* [1988]. The value given for the chosen model atomic oxygen density is in excellent agreement with the measured ratio of 0.14 ± 0.03 (Table 1). A re-evaluation of these calculations with the atmospheric and geometrical parameters corresponding to the present observations would be valuable.

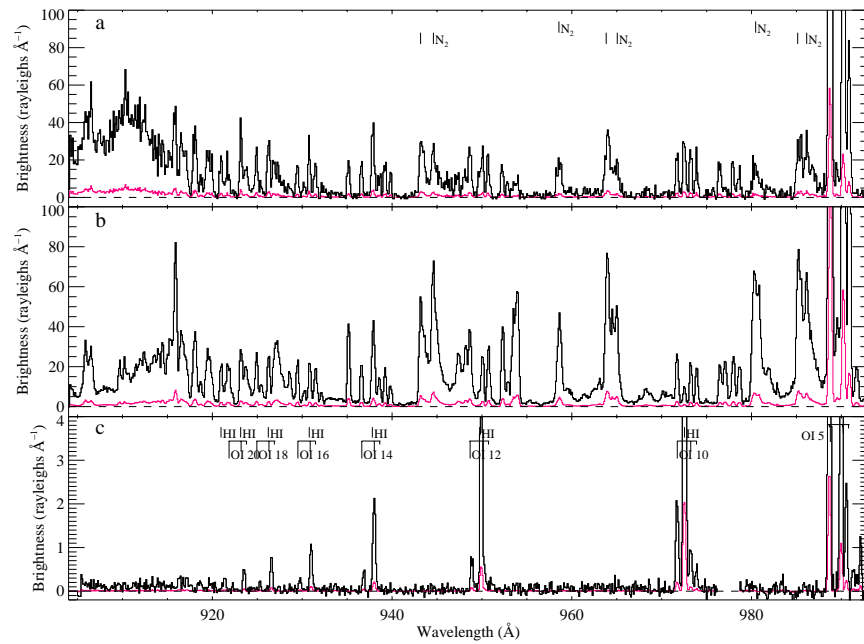


Figure 7. a) FUSE LWRS spectrum of the Earth limb, 904–994 Å, averaged over tangent heights from 250 to 500 km. b) LWRS disk spectrum of the same spectral range (see Figures 1 and 2). c) LWRS dayglow spectrum viewing at a zenith angle of $\sim 90^\circ$ from the 766 km spacecraft altitude.

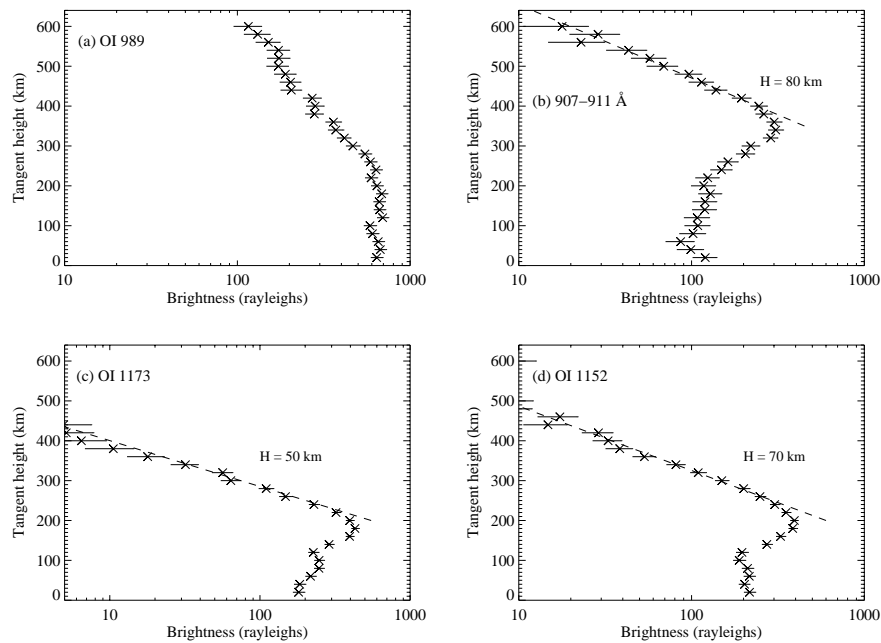


Figure 8. Extracted limb profiles of the $O^+ - e^-$ recombination continuum and selected atomic oxygen emissions. The dashed lines show arbitrarily scaled top side scale height profiles.

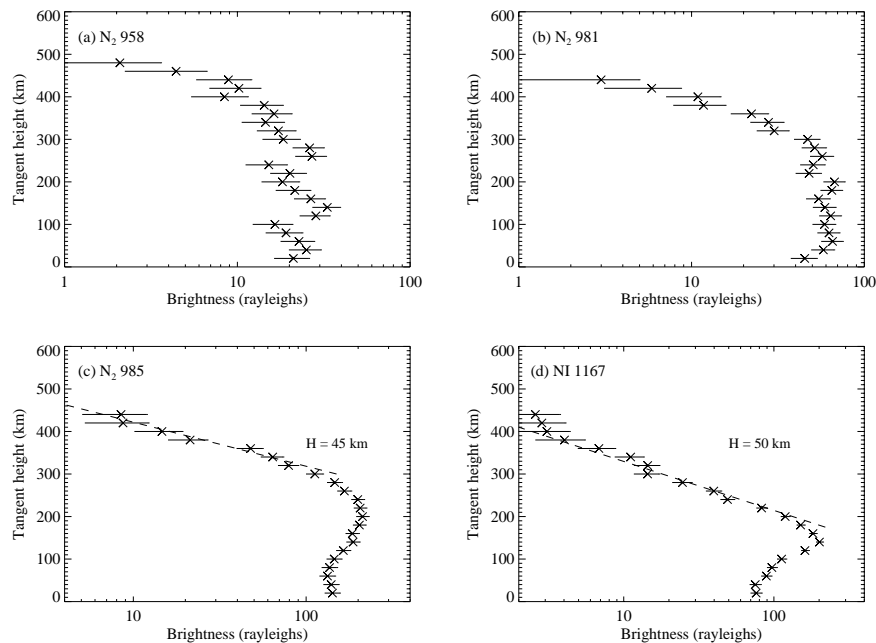


Figure 9. Extracted limb profiles of the N₂ Carroll-Yoshino (0,0), (0,1) and blended (3,4) and (4,5) bands, together with that of the optically thin atomic nitrogen emission at 1167 Å. The dashed lines show arbitrarily scaled top side scale height profiles.

O⁺ – e⁻ Recombination Continuum

The spatial profile of the O⁺ recombination continuum shown in Figure 8 was extracted by limiting the bandpass to wavelengths between 907 and 911 Å, so as to avoid contamination by the NI emissions near 906 Å. In addition, only data from the second through fourth orbits was summed as these showed the strongest recombination emission. Analysis of the spacecraft orbit indicates that these observations were made between magnetic latitudes 13–17° N, close to the middle of the Appleton anomaly, while in the later orbits, it was at higher magnetic latitude. Also, all of these limb profiles are from the dusk side, the dawn side showing no emission at all. This could be due to two factors: the dawn limb crossings were at magnetic latitudes between 7° S and 7° N, where the electron density is a minimum; the dawn electron densities are in general less than those at dusk.

The emission profile, Figure 8b, peaks near 350 km, in contrast to optically thin emissions produced by photoionization or photoelectron impact whose maxima are at lower altitudes. Recombination emission is expected to peak near the maximum in electron density which is typically between 300 and 400 km. The derived brightness is only a lower limit as the integration band was limited and, in any case, the FUSE spectrographs cut off well above 890 Å, where emission was still seen in the HUT data by *Feldman et al.* [1992]. Comparison with the HUT results indicates that this emission is brighter on the day limb than at night, again consistent with the diurnal variation of electron density near the F₂ maximum. The top side scale height of 80 km reflects the distribution of the product of electron and O⁺ ion densities, which are nearly equal in this altitude range and have typical daytime scale heights of ~150 km. Detailed modeling remains to be performed.

It would also be valuable to obtain similar FUSE spectra on the nightside limb.

N₂ Carroll-Yoshino Bands

The N₂ Carroll-Yoshino ($c_4' \ ^1\Sigma_u^+ - X \ ^1\Sigma_g^+$) system, particularly the (0,0) and (0,1) bands at 958 and 981 Å, respectively, have long been of interest because of their weak emission rate in the atmosphere despite having the largest laboratory N₂ excitation cross sections. Similar to the O I $\lambda 1173$ /O I $\lambda 989$ ratio problem discussed above, the (0,0) band photons are radiatively trapped in the N₂ atmosphere and either branch to other optically thin transitions or are lost to predissociation in the upper state. The (0,0) and (0,1) bands are both identified in the spectrum of Figure 2, together with a blend of the (3,4) and (4,5) bands at 985 Å, that should appear optically thin. Limb profiles of these three emission features are shown in Figure 9, together with the profile of the optically thin N I $\lambda 1167$ ($^2D^o - ^2F$) transition used as a surrogate for electron impact excitation of N₂. Stevens et al. [1994] have performed a complete radiative transfer analysis for the (0, v') bands and their calculations of horizontal intensities for conditions of solar maximum are in reasonable agreement with our limb profiles. However, a firm conclusion regarding the correct value of the predissociation fraction cannot be drawn without repeating the calculation for the solar conditions and viewing geometry of the FUSE observations.

CONCLUSION

We have obtained spectra of the terrestrial day airglow between 905 and 1184 Å with unprecedented spectral resolution and sensitivity using the Far Ultraviolet Spectroscopic Explorer. The spectra presented here are only a first look at an extremely rich data set that is able to resolve a number of long standing aeronomical problems. The resonance transitions of Ar I are unambigu-

ously identified as are previously unreported transitions between highly excited energy levels of O⁺. Several bands of the N₂ Carroll-Yoshino system, particularly the (0,0), (0,1) and (0,2) bands, are clearly seen. Limb profiles of the strongest emissions are obtained and can be compared with recent excitation models. The spectrum and the tangent height profile of the O⁺ + e⁻ recombination continuum below 911 Å are also obtained.

Acknowledgments.

We dedicate this paper to William G. Fastie (December 6, 1916 – July 14, 2000), who long ago introduced two of us (PDF and HWM) to the beauty of atmospheric spectroscopy. We thank R. R. Meier and J. E. Bishop for enlightening discussions. This work is based on data obtained for the Guaranteed Time Team by the NASA-CNES-CSA FUSE mission operated by the Johns Hopkins University. Financial support has been provided by NASA contract NAS5-32985.

References

- Ajello, J. M., G. K. James, B. O. Franklin, and D. E. Shemansky, Medium-resolution studies of extreme ultraviolet emission from N₂ by electron impact - Vibrational perturbations and cross sections of the $c_4' \ ^1\Sigma_u^+$ and $b' \ ^1\Sigma_u^+$ states, *Phys. Rev. A*, 40, 3524–3556, 1989.
- Ajello, J. M., G. K. James, and M. Ciocca, High resolution EUV emission spectroscopy of the N₂ $c' \ ^1\Sigma_u^+$ $v' = 3$ and 4 levels by electron impact, *J. Phys. B*, 31, 2437–2448, 1998.
- Budzien, S. A., P. D. Feldman, and R. R. Conway, Observations of the far ultraviolet airglow by the Ultraviolet Limb Imaging experiment on STS-39, *J. Geophys. Res.*, 99, 23,275–23,288, 1994.
- Chakrabarti, S., F. Paresce, S. Bowyer, R. Kimble, and S. Kumar, The extreme ultraviolet day airglow, *J. Geophys. Res.*, 88, 4898–4904, 1983.
- Christensen, A. B., R. W. Eastes, P. D. Feldman, and E. P. Gentieu, High-resolution dayglow O I 1304 Å and O I 989 Å rocket observations, *J. Geophys. Res.*, 87, 6317–6323, 1982.

- Cotton, D. M., G. R. Gladstone, and S. Chakrabarti, Sounding rocket observation of a hot atomic oxygen geocorona, *J. Geophys. Res.*, *98*, 21,651–21,657, 1993.
- Feldman, P. D., A. F. Davidsen, W. P. Blair, C. W. Bowers, S. T. Durrance, G. A. Kriss, H. C. Ferguson, R. A. Kimble, and K. S. Long, The spectrum of the tropical oxygen nightglow observed at 3 Å resolution with the Hopkins Ultraviolet Telescope, *Geophys. Res. Lett.*, *19*, 453–456, 1992.
- Feldman, P. D., et al., Ultraviolet spectroscopy of the terrestrial airglow with the Hopkins Ultraviolet Telescope, *Eos, Trans. AGU*, *72*, 207, 1991.
- Gentieu, E. P., P. D. Feldman, and R. R. Meier, Spectroscopy of the extreme ultraviolet dayglow at 6.5 Å resolution – Atomic and ionic emissions between 530 and 1240 Å *Geophys. Res. Lett.*, *6*, 325–328, 1979.
- Gentieu, E. P., P. D. Feldman, R. W. Eastes, and A. B. Christensen, Spectroscopy of the extreme ultraviolet dayglow during active solar conditions, *Geophys. Res. Lett.*, *8*, 1242–1245, 1981.
- Gladstone, G. R., UV resonance line dayglow emissions on earth and Jupiter, *J. Geophys. Res.*, *93*, 14,623–14,630, 1988.
- Gladstone, G. R., R. Link, S. Chakrabarti, and J. C. McConnell, Modeling of the O I 989-A to 1173-A ratio in the terrestrial dayglow, *J. Geophys. Res.*, *92*, 12,445–12,450, 1987.
- Hubert, B., J.-C. Gérard, D. M. Cotton, D. V. Bisikalo, and V. I. Shematovich, Effect of hot oxygen on thermospheric O I UV airglow, *J. Geophys. Res.*, *104*, 17,139–17,144, 1999.
- Kelly, R. L., *Atomic and ionic spectrum lines below 2000 Angstroms. Hydrogen through Krypton*, New York: American Institute of Physics (AIP), American Chemical Society and the National Bureau of Standards, 1987, 1987.
- Meier, R. R., Ultraviolet spectroscopy and remote sensing of the upper atmosphere, *Space Science Reviews*, *58*, 1–185, 1991.
- Meléndez-Alvira, D. J., R. R. Meier, J. M. Picone, P. D. Feldman, and B. M. McLaughlin, Analysis of the oxygen nightglow measured by the Hopkins Ultraviolet Telescope: Implications for ionospheric partial radiative recombination rate coefficients, *J. Geophys. Res.*, *104*, 14,901–14,914, 1999.
- Moos, H. W., et al., Overview of the Far Ultraviolet Spectroscopic Explorer Mission, *Astrophys. J.*, *538*, L1–L6, 2000.
- Morrison, M. D., and R. R. Meier, The O I 989 and 1173 Å multiplets in the dayglow, *Planet. Space Sci.*, *36*, 987–1003, 1988.
- Morrison, M. D., C. W. Bowers, P. D. Feldman, and R. R. Meier, The EUV dayglow at high spectral resolution, *J. Geophys. Res.*, *95*, 4113–4127, 1990.
- Morton, D. C., Atomic data for resonance absorption lines. I – Wavelengths longward of the Lyman limit, *Astrophys. J. (Supp.)*, *77*, 119–202, 1991.
- Parker, J. W., S. A. Stern, G. R. Gladstone, and J. M. Shull, The Spectroscopic Detectability of Argon in the Lunar Atmosphere, *Astrophys. J.*, *509*, L61–L64, 1998.
- Pettersson, S.-G., and I. Wenaker, Vacuum-ultraviolet lines in the spectrum of O II, *Physica Scripta*, *42*, 187–191, 1990.
- Roncin, J. Y., and F. Launay, Tables of vacuum ultraviolet emission band systems of molecular nitrogen from 82.6 to 124.2 nm, *Astron. Astrophys. (Supp.)*, *128*, 361–362, 1998.
- Sahnou, D. J., et al., On-Orbit Performance of the Far Ultraviolet Spectroscopic Explorer Satellite, *Astrophys. J.*, *538*, L7–L11, 2000.
- Shemansky, D. E., I. Kanik, and J. M. Ajello, Fine-Structure Branching in N₂ c₄¹Σ_u⁺(0), *Astrophys. J.*, *452*, 480–485, 1995.
- Stevens, M. H., R. R. Meier, R. R. Conway, and D. F. Strobel, A resolution of the N₂ Carroll-Yoshino (c₄¹ – X) band problem in the Earth’s atmosphere, *J. Geophys. Res.*, *99*, 417–433, 1994.